JACS
JOURNAL OF THE AMERICAN CHEMICAL SOCIETY

Article

What is hidden behind Schiff base hydrolysis? Dynamic covalent chemistry for precise capture of sialylated glycans

Yuting Xiong, Xiuling Li, Minmin Li, Haijuan Qin, Cheng Chen, Dongdong Wang, Xue Wang, Xintong Zheng, Yunhai Liu, Xinmiao Liang, and Guangyan Qing

J. Am. Chem. Soc., **Just Accepted Manuscript** • DOI: 10.1021/jacs.0c01970 • Publication Date (Web): 03 Apr 2020

What is hidden behind Schiff base hydrolysis? Dynamic covalent chemistry for precise capture of sialylated glycans

Yuting Xiong,[†,‡,⊥] Xiuling Li,[†,⊥] Minmin Li,[†,‡] Haijuan Qin,[§] Cheng Chen,[†] Dongdong Wang,[†] Xue Wang,[†] Xintong Zheng,[†] Yunhai Liu,[‡] Xinmiao Liang*,[†] Guangyan Qing*,[†]

[†]CAS Key Laboratory of Separation Science for Analytical Chemistry, Dalian Institute of Chemical Physics, Chinese Academy of Sciences, 457 Zhongshan Road, Dalian 116023, P. R. China

[‡]Jiangxi Province Key Laboratory of Polymer Micro/Nano Manufacturing Devices, East China University of Technology, 418 Guanglan Avenue, Nanchang 330013, P. R. China

[§]Research Centre of Modern Analytical Technology, Tianjin University of Science and Technology, Tianjin 300457, P. R. China

[⊥]These authors contributed equally

ABSTRACT: The aberrant expression of sialylated glycans (SGs) is closely associated with the occurrence, progression, and metastasis of various cancers, and sialylated glycoproteins have been widely used as clinical biomarkers for cancers. However, identification and comprehensive analysis of SGs is exceptionally complex, which urgently need innovative and effective method to capture SGs from biosample in prior to MS analysis. Here, we report that a novel dynamic covalent chemistry strategy based on Schiff base hydrolysis can be applied for the precise capture of the SGs. The prepared Glucopyranoside-Schiff base-modified silica gel displays extraordinary enrichment selectivity (even at the ratio of 1:5000 with interference), high adsorption capacity (120 $mg \cdot g^{-1}$), and satisfying enrichment recovery (95.5 %) towards sialylated glycopeptides, which contributes to a highly specific, efficient, mild and reversible SG capturing approach that can remarkably promote the development of glycoproteomics and sialic acid sensing devices, and can be considerably promising in cancer biomarker discovery. Meanwhile, the facile hydrolysis characteristic of our Schiff base material completely subverts conventional knowledge of enrichment materials, the chemical stability of which is usually regarded as a prerequisite. Importantly, we find an exciting story hidden behind the Schiff base hydrolysis reaction, which demonstrates the unique advantage of dynamic covalent chemistry in glycoproteomics and biomolecule sensing.

INTRODUCTION

Life runs on carbohydrates. Glycans, carbohydrate chains that are attached to the cell surface in the form of dense glycocalyx (Figure 1a), participate in and regulate a wide range of biological processes, including cell signaling, cell proliferation and migration.[1-3] *N*-acetyl-neuraminic acid (Neu5Ac, a type of sialic acid), is typically found at the outmost location of glycans.[4,5] Due to this prominent position and ubiquitous distribution, sialylated glycans (SGs) widely participate in physiological and pathological processes, such as tumour development and metastasis, pathogen infection, immune response and evasion.[6,7] Abnormal expression of SGs is a hallmark of the onset and progression of various cancers.[8,9] Moreover, the prevalence of one linkage form of SG over other linkages could help in determining the type of cancer. A study presented that human prostate cancer and gastric cancer exhibit an obvious increase in the expression of α-2,3-linked SGs.[10,11] To date, more than 20 glycoproteins have been approved as clinical cancer biomarkers by the US FDA, and the majority of them are sialylated.[12,13]

In addition, SGs play important roles in immune response and infection of human viruses.[14] For examples, SGs and high-mannose glycans on the envelop protein (GP120) of HIV-1 shield the virus from immune surveillance.[15,16] Cell surface SGs with a specific linkage also function as receptor determinants and mediate the entry of the Influenza viruses[17] and the Middle East respiratory syndrome coronavirus (MERS-CoV).[18] Therefore, the sialylation analyses, including the tasks of defining the sialylation sites and intact glycan structures, and deciphering their roles in the related bio-process, will facilitate the elucidation of the functions of glycoproteins or cells,[6] the discovery of novel disease biomarkers and drug targets,[12,13,19] and the development of antivirus drugs or vaccines.[20]

However, the extremely low abundance of many SGs, the strong interference from their counterparts, the dynamic nature of protein sialylation, the heterogeneity of glycan structures and the abundant linkage isomers pose a huge obstacle for the sialylation analysis.[4,21,22] Advances in mass spectrometry (MS)–based glycomics and glycoproteomics strongly rely on highly efficient and robust methods to capture the SGs from complex biosamples.[23] To date, hydrazide chemistry, a mainstreaming enrichment method based on covalent bonding, have been applied in glycoproteomic studies, which has a higher coverage for glycosylation sites[24,25] compared with other methods. However, the irreversible destruction of glycans arising from the violent oxidation conditions leads to the loss of information of the glycan structures, which is the most valuable resource.[26] In order to obtain intact glycan information, various affinity strategies, such as lectin affinity,[27] boronic acid affinity,[28,29] hydrophilic interaction liquid chromatography (HILIC),[30,31] and titanium dioxide[32,33] were developed. But their glycosylation site coverage and enrichment selectivity are not satisfying, the problems will be more difficult for the capture of cell-surface glycoproteins.[34,35] Therefore, there is an urgent and long-standing interest to develop innovative and effective capture methods for SGs to study protein glycosylation.[35-38]

In sharp contrast to the static affinity and irreversible covalent bonding strategies, dynamic covalent chemistry that deals with the reversible formation/cleavage of covalent bonds or the exchange of molecular components under equilibrium control,[39,40] arouses our great interest for its potential in the reversible glycan capture. Here we report an interesting finding that the hydrolysis reaction of dynamic imine bond (Schiff base) can be used to specifically capture SGs. As shown in Figure 1b, the Glucopyranoside-Schiff base-modified silica gel material (abbreviated as Glu-Schiff base@SiO_2) was prepared by

conducting an imine-formation reaction between 4-formylphenyl-D-glucopyranoside and (3-aminopropyl)-trimethoxysilane–modified silica gels (Scheme S1 in Supporting Information (SI)). The grafting percentage of Glu-Schiff base on SiO_2 was determined to be approximately 9 % in weight (Figure S1 in SI).

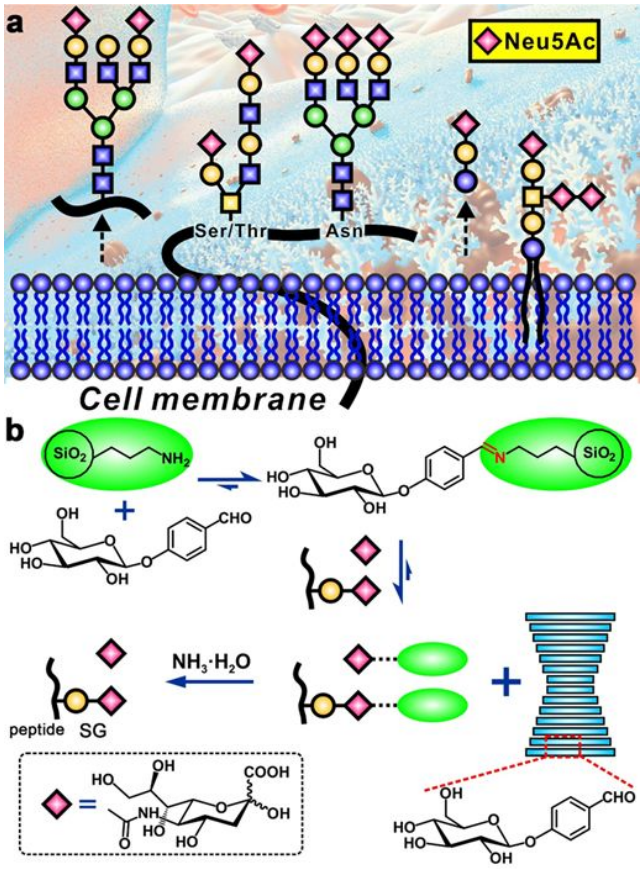

Figure 1. Significance of sialylated glycans (SGs) and the material design for the precise capture of SGs. (a) Mammalian cell surface is covered with a dense layer of glycocalyx (including glycoproteins, glycolipids, and glycoconjugates). In particular, the sialic acid–rich glycans are highly expressed on the cancer cell surfaces. The binding of these glycans with selectins on platelets and endothelial cell surfaces promotes the cancer cells to spread or metastasise. (b) Schematic illustration of a highly efficient capturing strategy for sialic acid or SGs based on the Schiff base hydrolysis reaction. Chemical structure of *N*-acetyl-neuraminic acid (Neu5Ac), a typical sialic acid, is shown using as purple ◆.

Benefiting from reversible covalent bonding and formation of unique SG–precursor amine complex, as well as an ordered self-assembly of the starting reagent Glu that further facilitates the hydrolysis reaction (Figure 1b), the Glu-Schiff base@SiO_2 material displays extraordinary sialylated glycopeptide (SGP) enrichment selectivity for both model protein sample and human serum, as well as high adsorption capacity and recovery towards the SGPs. The excellent performance of the material could not be explained by the typical HILIC mechanism simply. Moreover, the easily hydrolytic characteristic of our material subverts conventional knowledge of enrichment materials, in which the stability of the material is usually regarded as a prerequisite. Thus, a detailed analysis that discloses an intriguing story hidden behind the Schiff base hydrolysis is introduced in a step-wise manner by us.

RESULTS AND DISSCUSSION

SGP enrichment from model protein samples

First, the prepared Glu-Schiff base@SiO_2 were filled in micro solid phase extraction (SPE) columns. The enrichment selectivity of the material for SGPs was evaluated in a microscale SPE protocol[41] (Figure 2a, Table S1 in SI) by using the tryptic digestion of bovine fetuin (a standard glycoprotein) mixed with different molar ratios of bovine serum albumin (BSA) interference (e.g., 1:200 and 1:5000) as model protein samples. An optimum enrichment protocol was built by using 85% acetonitrile (ACN)/H_2O containing 1% formic acid (FA) as a peptide loading solution, 80% ACN/H_2O containing 1% FA as a washing solution and ammonia solution (10 % $NH_3 \cdot H_2O$) as an elution solution, respectively, the detailed optimization processes are described in Figure S2 in SI. It is worth noting that, in this protocol, the glycopeptides adsorbed on the material surface were eluted with 10 % $NH_3 \cdot H_2O$, which is completely different from the traditional glycopeptide elution procedures where the mixed solution of acetonitrile and water was usually used as the elution solution.[37,42] Based on the special protocol, 38 glycopeptide signals were identified by MS from the tryptic digestion of fetuin mixed with 200-fold BSA interference (Figure S3 in SI), and most signals belonged to the SGPs (Table S2 in SI). To our surprise, when a 5000-fold BSA interference was introduced, the identified number of the glycopeptides remained at the comparable level, 30 glycopeptides containing 21 SGPs (Figure 2b and Table S2 in SI) were identified by comparing the *m/z* value with that obtained in our previous works,[43-45] which was far superior to two commercial materials (ZIC-HILIC and Sepharose, as shown in Figure S4 and S5 in SI). Interestingly, we even identified 6 unknown glycopeptide signals (marked with red stars in Figure 2b) from the trace impurities in BSA,[45] illustrating the ultra-strong enrichment capacity of our material.

SGP enrichment from human serum

Furthermore, human serum was employed as an example[46] to assess the enrichment performance of Glu-Schiff base@SiO_2 in a complex biosample. Triplicate parallel experiments of glycopeptide enrichment were performed by using 100 μg of proteins extracted from human serum each time. Based on a similar optimized protocol described above, 283, 323 and 295 glycosites were identified in the three replicates (Figure 2c and Table S3 in SI), respectively. The localization of the *N*-glycosylation site was determined by a mass increase of 0.984 Da on the consensus sequence (N-X-S/T) (X≠P) after PNGase F deglycosylation. A false discovery rate of 1% was set for peptide identification and glycosylation site location. In addition, a dataset analysis (Figure 2d) reveals substantial overlapping between the identified glycopeptides among these replicates. In addition to the number of the identified glycosites, the glycopeptide enrichment selectivity also is a crucial parameter, which is defined as the ratio of the identified glycopeptides to the total number of peptides detected by the MS. An average enrichment selectivity of approximately 77 % was obtained for the analysis of the human serum sample. Moreover, the enrichment condition of our material was mild, and intact structural information of the glycans could be retained in comparison with the hydrazide chemistry method.

SGP adsorption capacity and recovery evaluation

The adsorption capacity of our material towards a standard SGP (CAS: 189035-43-6) was 120 $mg \cdot g^{-1}$ (Figure S6 in SI),

which was substantially higher than those of the commercial ZIC-HILIC (10 mg·g^{-1}) and Sepharose (10 mg·g^{-1}) (Figure 2e). The value (120 mg·g^{-1}) was also higher than those of two control materials Phenyl-Schiff base@SiO_2 (without β-D-glucopyranoside unit) (20 mg·g^{-1}) and NH_2@SiO_2 (without phenyl β-D-glucopyranoside) (10 mg·g^{-1}), their chemical structures are shown in Scheme S1 in SI. From the perspective of surface wettability, the Glu-Schiff base@SiO_2 surface was highly hydrophilic with a water contact angle (CA) of 20 ± 2°, which remarkably improved the approachability of the material surface for SGPs through hydrophilic interaction. While, the CAs of the Phenyl-Schiff base@SiO_2 and NH_2@SiO_2 surface were 71 ± 2° and 60 ± 2° (Figure S7in SI), respectively. These CA data indicated that the role of β-D-glucopyranoside in the Glu-Schiff base@SiO_2 material was very essential, and the hydrophilic SGPs were inclined to approach the highly hydrophilic Glu-Schiff base@SiO_2 surface.

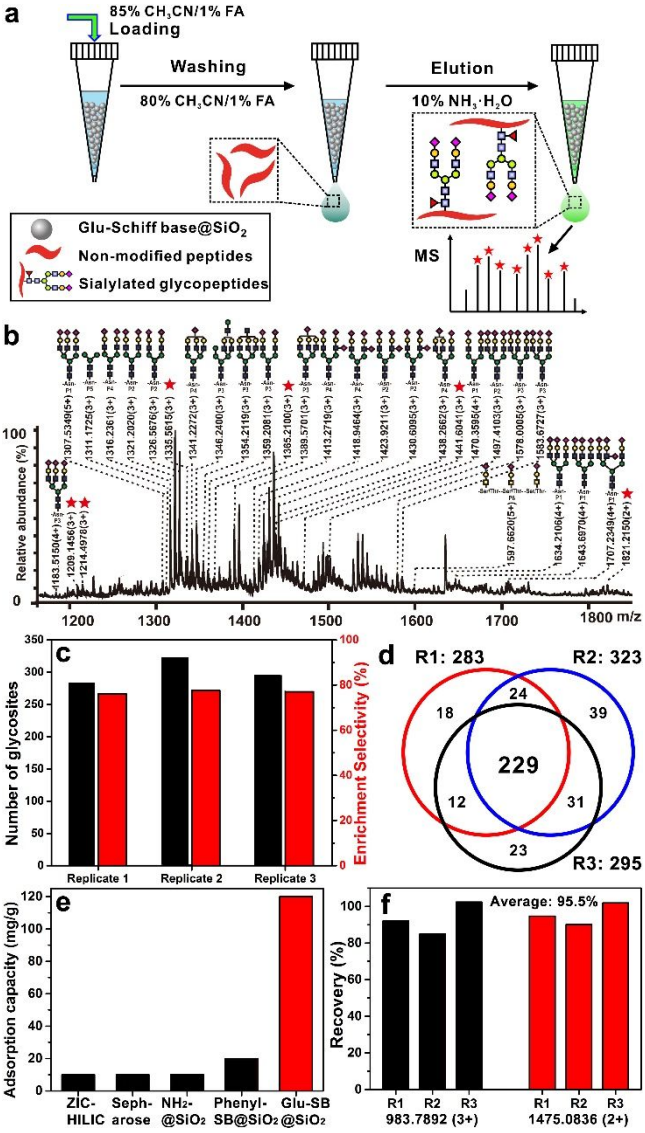

Figure 2. Sialylated glycopeptide (SGP) enrichment with the Glu-Schiff base@SiO_2 material. (a) The enrichment strategy based on a micro solid phase extraction protocol. (b) Mass spectrum (MS) of glycopeptides enriched with the Glu-Schiff base@SiO_2 obtained from the tryptic digestion of fetuin and BSA at a molar ratio of 1:5000. Glycopeptides are marked with red stars or their glycan structures: blue ■ : GlcNAc, green ● : mannose, yellow ● : galactose, and purple ◆ : Neu5Ac. (c) Glycopeptide enrichment from human serum with the Glu-Schiff base@SiO_2. Number of glycosites and the corresponding enrichment selectivity identified by MS. (d) Venn diagram of the identified glycopeptides from three replicated experiments. (e) Comparison among the adsorption capacity of ZIC-HILIC, Sepharose, NH_2@SiO_2, Phenyl-Schiff base@SiO_2 and Glu-Schiff base@SiO_2 towards a standard SGP (CAS: 189035-43-6). (f) Recovery of Glu-Schiff base@SiO_2 material–based enrichment method towards two SGPs [*m/z*: 983.7892 (3+) and 1475.0836 (2+)], obtained from three parallel MS measurements.

Moreover, the high SGP adsorption capacity under the loading condition and the strong desorption ability under the ammonia elution endowed the Glu-Schiff base@SiO_2 material with an additional merit of satisfactory controllability for the SGP adsorption and desorption, contributing to a high recovery. Here, the recovery is defined as the ratio of the released glycopeptide to the total glycopeptide loaded onto the enrichment materials. The Glu-Schiff base@SiO_2 material exhibited a high recovery rate of 95.5% towards two typical SGPs (Figure 2f and Table S4 in SI), which was comparable to the recovery rate obtained by the hydrazide chemistry method.[47] The merit makes our material particularly suitable for the capture and analysis of SGPs, which will facilitate a series of interesting applications in sialic acid sensing, cell surface sialylation profiling,[48] tumour cell sorting,[11] and early diagnosis of various cancers.[12,13]

Neu5Ac–triggered Schiff base hydrolysis

An interesting question arises, why does the Glu-Schiff base@SiO_2 material show the ultra-strong affinity towards SGs? To answer this question, two model molecules, Neu5Ac (the outmost molecule of SGPs) and 4-[(phenethylimino)methyl]phenyl-D-glucopyranoside (abbreviated as Schiff base **A** in Figure 3a, Scheme S2 in SI) that is the core component of the Glu-Schiff base@SiO_2 material, were introduced. The Schiff base **A** was hydrolyzed slowly[49] into phenylethanamine (PEA) and 4-formylphenyl β-D-gluco-pyranoside (abbreviated as **B**) in water (Figure S9a–9c in SI). When an equimolar Neu5Ac was added, remarkable changes in ^{1}H NMR spectra and strong exothermic response (33 μcal·s^{-1}) were observed (Figure S9d and S10 in SI), which indicated that Neu5Ac triggered Schiff base **A** hydrolysis[50] and strong interactions[51] between Neu5Ac and the hydrolysates might occur.

A stable SG–precursor amine complex produced upon the Schiff base hydrolysis

To identify the reaction products of the Schiff base hydrolysis in the presence of Neu5Ac, a separation procedure was conducted on a home-made Click TE-Cys hydrophilic column.[52] As shown in Figure 3b, the sharp peak at retention time of 11 min was observed and identified to be 4-formylphenyl β-D-glucopyranoside **(B)** by analyzing the retention time and ^{1}H NMR spectrum (Figure S11 and S12 in SI). A new peak at 17.5 min gave a *m/z* value of 431.2032, as shown in Figure 3c [($M+H^+$), the corresponding formula was calculated as $C_{19}H_{30}N_2O_9$ with a molecular weight (mw) of 430.2], which attracted our special attention. Furthermore, in the MS/MS spectrum (the inset of Figure 3c), two ions at *m/z* 274.0917 and 122.0962 were determined from the characteristic fragment of Neu5Ac (mw: 309.2) and from the PEA (mw: 121.1), respectively. This implied that a Neu5Ac–PEA complex might be produced upon the Schiff base hydrolysis reaction.

The chemical structure of the possible PEA–Neu5Ac complex was further characterised using ^{1}H, ^{13}C and ^{1}H–^{13}C COSY NMR spectra (Figure S13 and S14 in SI). The ^{13}C NMR spectra (Figure 3f) show that all characteristic peaks of both PEA (Figure 3d) and Neu5Ac (Figure 3e) were still observed. In particular, the tag group phenyl could be observed clearly, as indicated by the amplified ^{1}H–^{13}C COSY NMR spectrum (Figure 3g). Nevertheless, some carbons that belong to either PEA or Neu5Ac display evidential changes in chemical shift, the most obvious changes are contributed from C-1, C-2, C-3, and C-7 of Neu5Ac and C-10, C-11, and C-12 of PEA (Figure 3f).

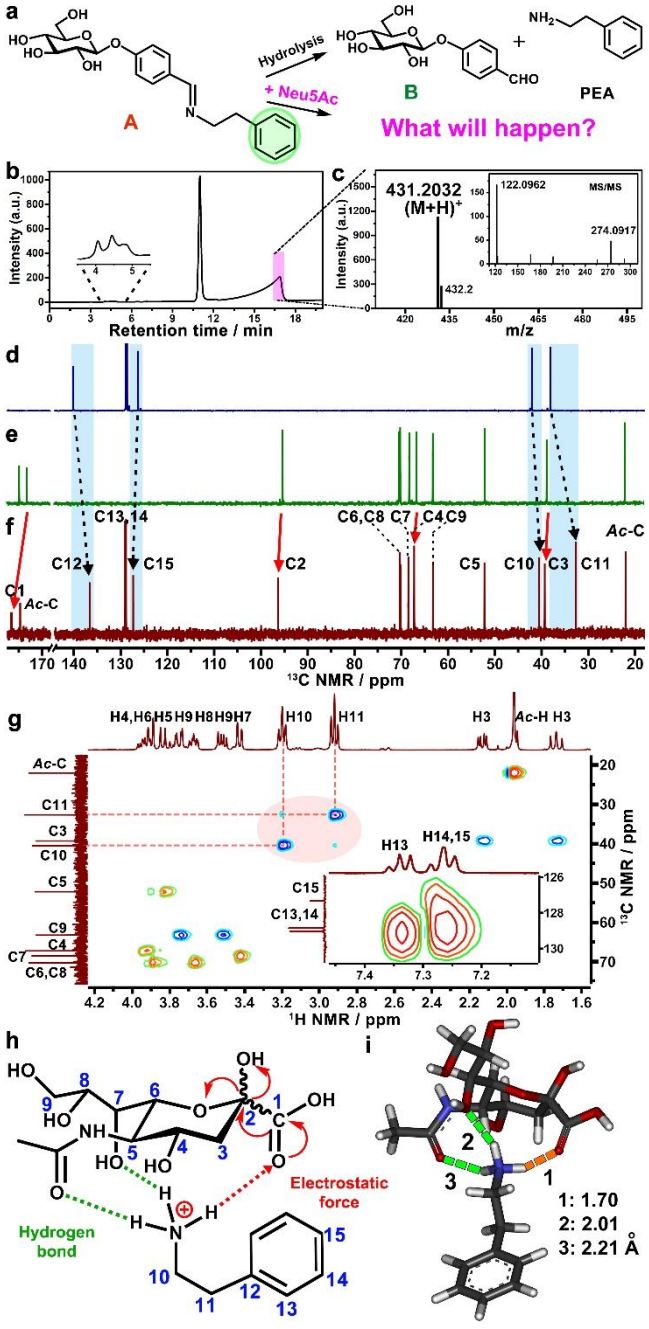

Figure 3. A stable SG–precursor amine complex produced upon the Schiff base hydrolysis. (a) Schematic illustration of the hydrolysis reaction of Schiff base **A** and the core topic of this study–what happened to the Schiff base **A** when it encountered Neu5Ac in aqueous solution. (b) High performance liquid chromatography (HPLC) diagram of the reaction product of the Schiff base hydrolysis based on a home-made semi-preparative liquid chromatography column (Click TE-Cys). Solvent gradient: a linear gradient of 90%−50% acetonitrile over 20 min at a flow rate of 3 mL·min^{-1}. (c) MS and MS/MS (the inset of c) of the PEA–Neu5Ac complex. (d–f) ^{13}C nuclear magnetic resonance (NMR) spectra of PEA (d), Neu5Ac (e) and PEA–Neu5Ac complex (f). (g) ^{1}H–^{13}C COSY NMR spectra of the PEA–Neu5Ac complex (Solvent: D_2O and temperature: 20°C). (h) Chemical structure of a possible binding mode between PEA and Neu5Ac, and the assignment of each C atom and H proton is shown in the NMR spectra. (i) A possible binding model of PEA–Neu5Ac complex obtained by quantum chemistry calculation (Gaussian, density function theory (DFT) at 6-311g level), water was set as the solvent. Electrostatic force and hydrogen bonding interactions are indicated by orange and green dashed lines with different lengths, respectively.

Based on the above results, the formation of the PEA–Neu5Ac complex was confirmed (Figure 3h), and their binding model was verified by a quantum chemistry calculation (Gaussian) (Figure 3i and Figure S15 in SI). The complexation relied on the strong attractive electrostatic force between the positively charged amine in PEA and the carboxylic acid in Neu5Ac. Meanwhile, two sets of hydrogen bonds formed between the amine in PEA and the –OH at C-7 position and the carbonyl of the acetyl group in Neu5Ac, which further strengthened the complexation. Note that the complexation was highly efficient, because most PEA interacted with Neu5Ac to form a stable complex, only a small amount of free PEA was found in the chromatogram of the products (amplified peak around 4.5 min in Figure 3b).

In addition, the acidic role of Neu5Ac in the Schiff base hydrolysis was studied by using octanoic acid as an alternative of Neu5Ac. ITC and MS results revealed that the hydrolysis of Schiff base **A** also occurred upon the addition of octanoic acid (Figure S16a in SI). But, the stable complex between octanoic acid and the released PEA was not observed in the MS (Figure S16b in SI). This result indicated that the acidity of Neu5Ac played a key role for the hydrolysis, [53] and formation of the PEA–Neu5Ac complex indeed relied on multiple interactions between the released PEA with multiple groups of Neu5Ac. This also reflected the high specificity of the Schiff base material toward the Neu5Ac.

Furthermore, to better mimic the SGs, Neu5Acα(2-3)GalβMP glycoside (abbreviated as NGg), a sialylated disaccharide, was selected as the model glycan to study the Schiff base hydrolysis and the corresponding formation of the complex. The binding model of PEA and NGg (Figure S17-S19 in SI) was found to be consistent with PEA–Neu5Ac binding. And, the core structure remained the high-affinity binding of the Neu5Ac unit in NGg with the hydrolysate PEA of the Schiff-base **A**. Based on these analyses, we presumed that the formation of this core binding structure (Figure 3h) was the key factor for the high affinity of the Glu-Schiff base@SiO_2 material to SGPs.

Self-assembly property of the hydrolysates

The Neu5Ac-triggered hydrolysis of the Schiff base **A** produced two products, the PEA–Neu5Ac complex, and 4-formylphenyl β-D-glucopyranoside (**B**). Interestingly, we found that **B** had a strong self-assembly capacity in water,[54] which would promote the hydrolysis reaction,[55] and facilitate the complexation of the hydrolysate PEA with Neu5Ac.

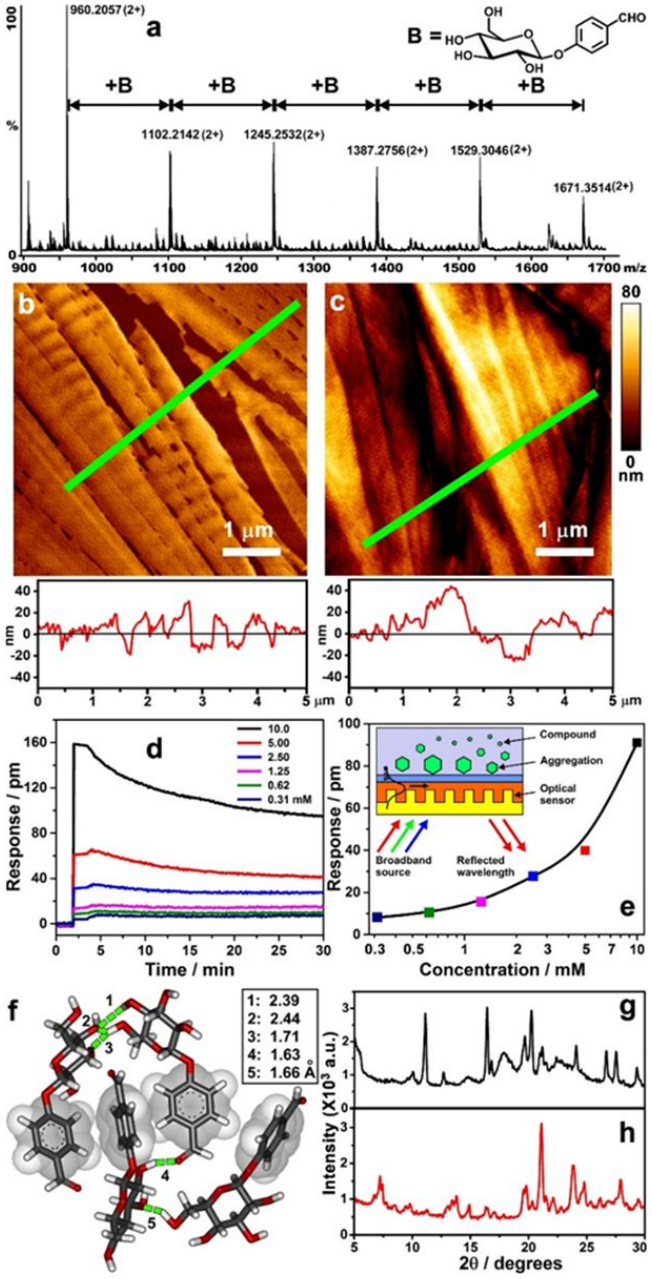

Figure 4. Self-assembly of 4-formylphenyl β-D-glucopyranoside (**B**). (a) High-resolution MS spectrum of the reaction mixture, a series of periodic MS signals are observed. (b, c) Atomic force microscopy (AFM) images of the mica surface after a deposition process of the reaction mixture of Schiff base **A** and Neu5Ac (b) or the individual **B** solution (c, 5 mM), and the corresponding section profiles of AFM images along the green lines. (d) Optical responsive curves of **B** molecule at different concentrations in H_2O monitored by a Corning® Epic® system. (e) Concentration-dependent responsive curve; plots were generated using the response values at 30 min. Inset shows a detection mechanism of the system. (f) A possible stacking model of the **B** molecule, π–π stacking between adjacent phenyl rings is indicated by grey electronic clouds, while hydrogen bonds are indicated by green dashed lines with different lengths. (g, h) Small angle X-ray diffractometer (XRD) spectra of the freeze-dried sample collected from the self-assembled **B** solution (g) or from the reaction mixture of Schiff base **A** and Neu5Ac (h). Sample amount: 30 mg, XRD spectra were recorded in the range of 2θ=5–30° at a scan rate of 0.05 °/s.

Specifically, a series of regular MS peaks with a same *m/z* difference value of approximately 142 (with two positive charges, mw difference = 142 × 2, corresponding to **B** molecule) were observed in a *m/z* range from 900 to 1700 (Figure 4a), by analyzing the reaction mixture using high-resolution MS, implying that **B** might form a series of self-assembled aggregations.[56] Subsequently, a piece of freshly cleaved mica was immersed in the reaction mixture, allowing the self-assembly to deposit on the mica surface. The self-assembly produced a large number of long ribbons with an average height of 20 nm (Figure 4b and Figure S20a in SI), as observed by atomic force microscopy (AFM). Similarly, individual **B** (5 mM) could also self-assemble into a similar ribbon-like structure (Figure 4c and Figure S20b in SI). Then, the aggregation assay procedure was conducted to detect the formation of self-assembly on the surface of a biosensor using a label-free Corning® Epic® technology (Figure 4d). The addition of **B** led to a large change in the refractive index of the sensor,[57] which showed a clear dose-dependent response at 30 min, giving a critical aggregation concentration of 1.25 mM in H_2O (Figure 4e and Figure S21 in SI). ^{1}H NMR titration (Figure S22 in SI) further validated the self-assembled behaviour.[58]

Quantum chemistry calculation (Gaussian, DFT) describes a possible stacking model of four **B** molecules (Figure 4f). In the model, four phenyl groups align along the X-axis via π–π stacking, and two glucopyranoside groups from the 1st **B** and the 3rd **B** interact with each other through multiple hydrogen bonding interactions. The multiple sharp peaks in the small angle X-ray diffractometer (XRD) spectrum of the self-assembly from the individual **B** (Figure 4g) demonstrated the long-range molecular packing and high crystallinity of the self-assembly.[59] Compared with the individual **B**, although the crystallinity of the newly born **B** in the hydrolysis reaction mixture decreased, the aggregation remained ordered (Figure 4h). The self-assembled structure might contain multiple stacking modes.

A possible reaction mechanism

Based on the above results, a possible reaction mechanism was proposed to elucidate what was hidden behind the Schiff base hydrolysis, as illustrated in Figure 5. The tag group phenyl represented a silica gel surface. First, Schiff base **A** was synthesised through a nucleophilic addition between PEA and **B**, and the subsequent elimination of a water molecule, in an anhydrous ethanol under a mild alkaline condition with triethylamine.[60] When the Schiff base **A** was dissolved in water, the hydrolysis reaction occurred slowly to generate PEA and **B**, which represented the intrinsic nature of the dynamic imine bond.[61] Upon addition of the hydrophilic Neu5Ac or SG, the hydrophilic interaction drove these components to approach the hydrophilic surface[62] of the Schiff base material. Such sufficient contact further activated the hydrolysis reaction of Schiff base **A**. On the one hand, the released PEA could form a stable complex with Neu5Ac or SG through strong electrostatic force and multiple hydrogen bonding interactions, which in turn promoted the hydrolysis reaction. On the other hand, the newly born **B** exhibited a strong self-assembly ability, and the occurrence of the self-assembly accelerated the hydrolysis reaction. These two driving forces together facilitated the decomposition of imine bonds of Schiff base **A**, thus resulting in a rapid kinetic reaction.

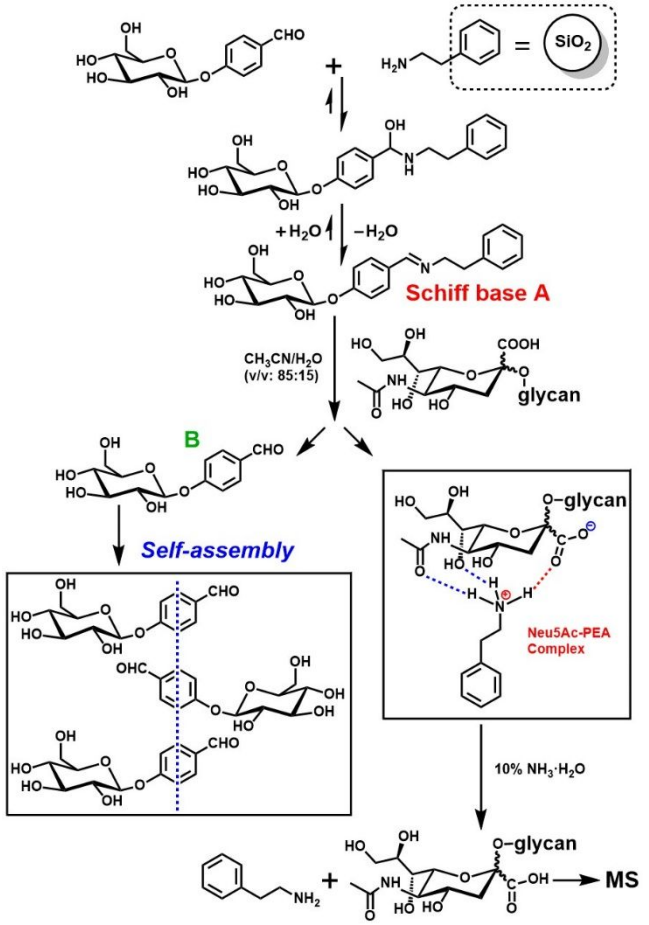

Figure 5. A possible reaction mechanism presenting the high affinity of the Glu-Schiff base@SiO_2 towards Neu5Ac residue or SG. In this study, a phenyl ring was introduced as a tag to mimic the SiO_2 microsphere, and for the convenience of structural characterisation.

Due to the supports of two sets of hydrogen bonding interactions and the strong electrostatic force, the PEA–Neu5Ac complex formed on the silica gel surface could not be destroyed and eluted by the conventional gradient elution readily. This finding explained the ultra-strong retention behavior of SG on the material surface. As a consequence, the PEA–Neu5Ac complex could be destroyed with 10 % $NH_3 \cdot H_2O$ through an amine exchanging reaction, thus the released Neu5Ac could be detected by MS.

Tracking the hydrolysis reaction using ^{15}N isotope labelled PEA

An ^{15}N isotope labelled PEA (denoted as ^{15}N-PEA) was selected as the reactant to prepare the Schiff base **A'**, and the chemical shift variation of the N atom in PEA was monitored by ^{15}N NMR in DMSO-d_6.[63] Figure 6a shows the ^{15}N NMR spectrum of the Schiff base **A'**. According to the result of quantum chemistry calculation, the signal at 324 ppm is assigned to C=N, and the other signal at 84 ppm is assigned to the –NH–CH(OH)– of an intermediate product of the Schiff base **A'** hydrolysis.[64] The free ^{15}N-PEA exhibited a characteristic N signal at 24 ppm (Figure 6b). When the Schiff base **A'** was mixed with an equimolar amount of Neu5Ac, the initial characteristic signals corresponding to the Schiff base **A'** disappeared, and a new signal appeared at 119 ppm (Figure 6c). In addition, the purified ^{15}N-PEA–Neu5Ac complex (obtained through a HPLC separation process) also exhibited a characteristic signal at 119 ppm in the ^{15}N NMR spectrum (Figure 6d), which was consistent with the signal observed in the reaction mixture. The results clearly illustrated the occurrence of the Schiff base hydrolysis and the formation of the PEA–Neu5Ac complex.

The configurational differences between the PEA–Neu5Ac complex and the PEA–Neu5Ac mixture

To prove the necessity of the Schiff base hydrolysis reaction, their configurational differences were investigated through surface enhanced Raman spectroscopy (SERS) by utilizing the 4-mercapto-phenyl boronic acid (MPBA)-modified silver nanoparticle (AgNPs) as both a Raman reporter and a Neu5Ac acceptor.[65] As the SERS spectrum of MPBA-modified AgNPs shown in Figure 6f, the peaks at 1585 cm^{-1} and 1574 cm^{-1} are ascribed to the totally symmetric vibrational mode and non-totally symmetric vibrational mode of the benzene ring of MPBA, respectively.[66] For MPBA-modified AgNPs, the intensity ratio of the peak at 1585 cm^{-1} to the peak at 1574 cm^{-1} (I_{1585}/I_{1574}) was approximately 0.998. When the PEA–Neu5Ac complex solution (10 mM) were incubated with MPBA-modified AgNPs, the SERS peak intensity at 1585 cm^{-1} decreased slightly (red line in Figure 6f), giving an I_{1585}/I_{1574} ratio of 0.969. In contrast, the addition of the PEA–Neu5Ac mixture (10 mM) led to an obvious decrease of the peak at 1585 cm^{-1} (blue line). Moreover, the I_{1585}/I_{1574} ratio decreased to 0.915, which indicated that a larger number of Neu5Ac molecules were captured by MPBA.

Kataoka *et al.* point out that phenylboronic acid has two binding patterns with Neu5Ac.[67] The major binding pattern relies on the covalent bonding between phenylboronic acid and *cis*-diols at the C-7 and C-8 positions of the majority of Neu5Ac with the help of the intramolecular coordination bond from the amide group, which was adopted by the binding between MPBA and the PEA–Neu5Ac mixture (as shown in Figure 6h), companied by a relatively larger decrease in the Raman signal ratio.

In addition, the aforementioned analyses on the structure of PEA–Neu5Ac complex clearly indicated that the C-7 OH and the amide group of Neu5Ac participated in the complexation with PEA. Because the C-7 OH was occupied in the PEA–Neu5Ac complex, only a labile binding of MPBA with the Neu5Ac unit of the PEA–Neu5Ac complex was achieved through the minor binding pattern that involved *cis*-diols at the C-8 and C-9 positions (Figure 6i). This result was consistent with the small variation in the Raman signal ratio. Moreover, a new Raman peak appeared at 648 cm^{-1} only when the PEA–Neu5Ac complex was introduced (Figure 6g), which was assigned to the stretching vibrations of C–N and C–C bonds in PEA.[68] This finding indicated that, compared with the PEA–Neu5Ac mixture, the PEA component from the PEA–Neu5Ac complex was much closer to the AgNPs surface due to the intensive binding between PEA and Neu5Ac.

^{1}H–^{13}C COSY NMR spectra provided additional evidence for the configurational difference between the PEA–Neu5Ac complex and their mixture (Figure S23 in SI) in D_2O. Moreover, ^{15}N NMR spectra (Figure 6e) indicated that the N signal (at 119 ppm) of the PEA–Neu5Ac complex was remarkably different from that observed from the PEA–Neu5Ac mixture (at 36 ppm). By taking the results of the SERS, ^{1}H–^{13}C, ^{15}N NMR spectra and other evidence (Figure S24-26 in SI) together, we concluded that the Schiff base hydrolysis reaction upon

encountering Neu5Ac could produce a highly stable PEA–Neu5Ac complex, which could not be accomplished by the direct mixing of PEA and Neu5Ac.

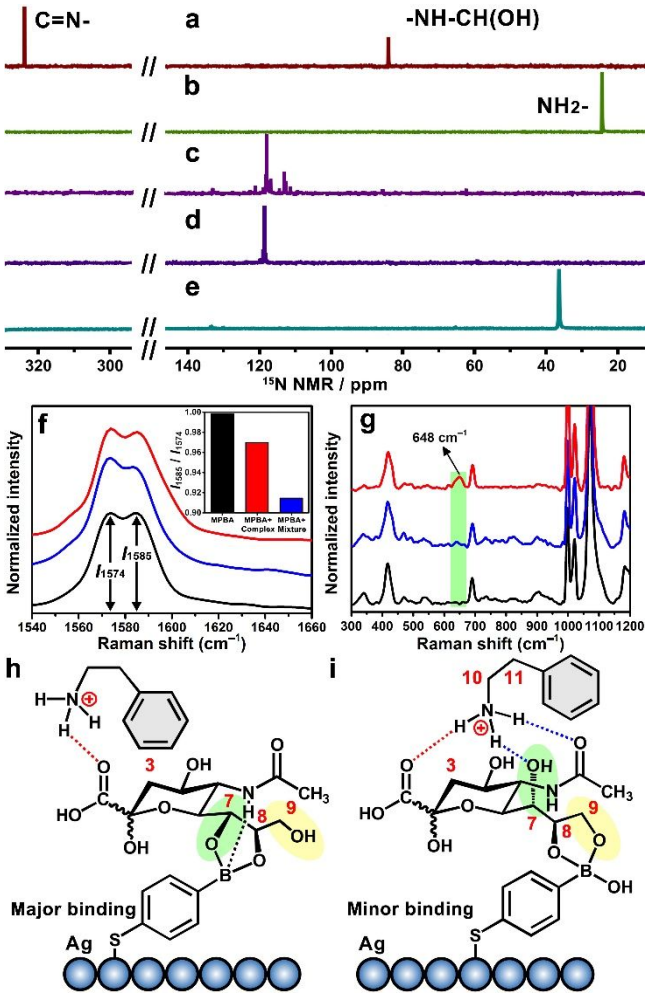

Figure 6. Investigation of the configurational difference between the PEA–Neu5Ac complex and the PEA–Neu5Ac mixture. (a–e) ^{15}N NMR spectra of Schiff base **A** (a), PEA (b), reaction mixture (c), the PEA–Neu5Ac complex (d) and the PEA–Neu5Ac mixture (e) in DMSO-d_6 at 20 °C (sample amount: 20 mg). (f, g) Amplified Raman spectra of 4-mercaptophenyl boronic acid (MPBA)-modified silver nanoparticles (AgNPs) surface before (black) and after being incubated with the solution of PEA–Neu5Ac complex (red) or PEA–Neu5Ac mixture (blue) (concentration: 10 mM, solvent: water). The inset of (f) shows the comparison among the Raman intensity ratios of the peak 1585 cm^{-1} to 1574 cm^{-1}. (h, i) Schematic illustration of the possible binding modes of the 4-MPBA-modified AgNPs surface interacted with PEA–Neu5Ac mixture (h) or PEA–Neu5Ac complex (i). The core binding groups are indicated by the green and yellow circles.

CONCLUSIONS

In summary, we reported a Schiff base hydrolysis–based dynamic chemistry strategy for the SG-specific capture. This strategy is remarkably different from the conventionally static binding affinity strategies. The formation of the PEA–Neu5Ac complex is highly stable and cannot be destroyed by increasing the solvent polarity. Benefiting from this feature, SGPs can be easily and efficiently isolated from non-modified peptides, thus contributing to a highly specific SGP enrichment method, the presented enrichment performance is comparable to the mainstream hydrazine chemistry method. Importantly, the glycans structure information remains intact due to the mild elution process with an ammonia solution. Thus, it is confidently believed that this method is considerably promising in the fields of glycoproteomics and glycobiology.[35] By using the method, more novel SGPs and sialylation sites could be identified efficiently from complex biosamples, thus largely deepening the understanding of SG-related cellular biological events, especially cancers and immune response.[23]

From the perspective of material sciences, our design strategy breaks the classical knowledge for enrichment materials, in which the chemical stability of the materials is usually regarded as the premise. In contrast, the Glu-Schiff base@SiO_2 material functions as a self-sacrificed reagent. The adsorption of SGs triggered the Schiff base hydrolysis reaction, only through which the PEA–Neu5Ac complexes could be generated. This study discloses the necessity of the Schiff base hydrolysis reaction and illustrates the considerable potential of the dynamic covalent chemistry strategy in the capture of target biomolecules.[69] The chemoselectivity and specificity of the capturing method might be improved remarkably due to the inherent merits of the chemical reaction.[40]

ASSOCIATED CONTENT

Supporting Information.
Materials and instruments, the synthesis and preparation procedures, characterization data, all experimental details, and supplementary figures and tables. This material is available free of charge via the Internet at http://pubs.acs.org.

AUTHOR INFORMATION

Corresponding Author

*qinggy@dicp.ac.cn
*liangxm@dicp.ac.cn

ORCID

Guangyan Qing: 0000-0002-4888-9318
Xinmiao Liang: 0000-0001-5802-1961

Notes

The authors declare no competing financial interest.

ACKNOWLEDGMENT

This work was supported by the National Natural Science Foundation of China (51473131, 21775116, 21922411 and 21934005), DICP Innovation Funding (DICP-RC201801) and LiaoNing Revitalization Talents Program (XLYC1802109). G. Qing acknowledges valuable discussion with Prof. Dr. Yonggui Zhou and Dr. Song Shi in DICP. The authors are thankful for Technique Supporting Platform for Clean Energy Research Division -DICP for their technical support.

REFERENCES

(1) Hart, G. W.; Copeland, R. J. Glycomics hits the big time. *Cell* **2010**, *143*, 672-676.

(2) Cummings, R. D.; Pierce, J. M. The challenge and promise of glycomics. *Chem. Biol.* **2014,** *21*, 1-15.

(3) Feizi, T. E.; Haltiwanger, R. S. Editorial overview: carbohydrate-protein interactions and glycosylation: glycan synthesis and recognition: finding the perfect partner in a sugar-coated life. *Curr. Opin. Struct. Biol.* **2015**, *34*, vii-ix.

(4) Varki, N. M.; Varki, A. Diversity in cell surface sialic acid presentations: implications for biology and disease. *Lab. Invest.* **2007**, *87*, 851-857.

(5) Schauer, R. Sialic acids as regulators of molecular and cellular interactions. *Curr. Opin. Struct. Biol.* **2009,** *19*, 507-514.

(6) Varki, A. Sialic acids in human health and disease. *Trends Mol. Med.* **2008**, *14*, 351-360.

(7) Reily, C.; Stewart, T. J.; Renfrow, M. B.; Novak, J. Glycosylation in health and disease. *Nat. Rev. Nephrol.* **2019,** *15*, 346-366.

(8) RodrÍguez, E.; Schetters, S. T. T.; van Kooyk, Y. The tumour glyco-code as a novel immune checkpoint for immunotherapy. *Nat. Rev. Immunol.* **2018,** *18*, 204-211.

(9) Ghosh, S. Sialic acids: biomarkers in endocrinal cancers. *Glycoconjugate J.* **2015**, *32*, 79-85.

(10) Pinho, S. S.; Reis, C. A. Glycosylation in cancer: mechanisms and clinical implications. *Nat. Rev. Cancer* **2015**, *15*, 540-555.

(11) Gilģunn, S.; Conroy, P. J.; Saldova, R.; Rudd, P. M.; O'Kennedy, R. J. Aberrant PSA glycosylation—a sweet predictor of prostate cancer. *Nat. Rev. Urol.* **2013**, *10*, 99-107.

(12) Stowell, S. R.; Ju, T.; Cummings, R. D. Protein glycosylation in cancer. *Annu. Rev. Pathol.: Mech. Dis.* **2015**, *10*, 473-510.

(13) Peracaula, R.; Barrabés, S.; Sarrats, A.; Rudd, P. M.; de Llorens, R. Altered glycosylation in tumours focused to cancer diagnosis. *Dis. Markers* **2008**, *25*, 207-218.

(14) Schwegmann-Wessels, C; Herrler, G. Sialic acids as receptor determinants for coronaviruses. *Glycoconjugate J.* **2006**, *23*, 51-58.

(15) Cao, L. W.; Diedrich, J. K.; Kulp, D. W.; Pauthner, M.; He, L.; Park, S. K. R.; Sok, D.; Su, C. Y.; Delahunty, C. M.; Menis, S.; Andrabi, R.; Guenaga, J.; Georgeson, E.; Kubitz, M.; Adachi, Y.; Burton, D. R.; Schief, W. R.; Yates, J. R.; Paulson, J. C. Global site-specific N-glycosylation analysis of HIV envelope glycoprotein. *Nat. Commun.* **2017**, *8*, 14954.

(16) Stewart-Jones, G. B. E.; Soto, C.; Lemmin, T.; Chuang, G. Y .; Druz, A.; Kong, R.; Thomas, P. V.; Wagh, K .; Zhou, T. Q.; Behrens, A. J.; et al. Bylund, T.; Choi, C. W.; Davison, J. R.; Georgiev, I. S.; Joyce, M. G.; Do Kwon, Y.; Pancera, M.; Taft, J.; Yang, Y. P.; Zhang, B. S.; Shivatare, S. S.; Shivatare, V. S.; Lee, C. C. D.; Wu, C. Y.; Bewley, C. A.; Burton, D. R.; Koff, W. C.; Connors, M.; Crispin, M.; Baxa, U.; Korber, B. T.; Wong, C. H.; Mascola, J. R.; Kwong, P. D. Trimeric HIV-1-env structures define glycan shields from clades A, B, and G. *Cell* **2016**, *165*, 813-826.

(17) Shinya, K.; Ebina, M.; Yamada, S.; Ono, M.; Kasai, N.; Kawaoka, Y. Influenza virus receptors in the human airway. *Nature* **2006**, *440*, 435-436.

(18) Li, W. T.; Hulswit, R. J. G.; Widjaja, I.; Raj, V. S.; McBride, R.; Peng, W. J.; Widagdo, W.; Tortorici, M. A.; van Dieren, B.; Lang, Y.; van Lent, J. W. M.; Paulson, J. C.; de Haan, C. A. M.; de Groot, R. J.; van Kuppeveld, F. J. M.; Haagmans, B. L.; Bosch, B. J. Identification of sialic acid-binding function for the Middle East respiratory syndrome coronavirus spike glycoprotein. *Proc. Natl. Acad. Sci. U. S. A.* **2017,** *114,* E8508-E8517

(19) Dube, D. H.; Bertozzi, C. R. Glycans in cancer and inflammation–potential for therapeutics and diagnostics. *Nat. Rev. Drug Discovery* **2005**, *4*, 477-488.

(20) Balzarini, J. Targeting the glycans of glycoproteins: a novel paradigm for antiviral therapy. *Nat. Rev. Microbiol.* **2007**, *5*, 583-597.

(21) Nie, H.; Li, Y.; Sun, X. L. Recent advances in sialic acid-focused glycomics. *J. Proteomics* **2012**, *75*, 3098-3112.

(22) Deng, L. Q.; Chen, X.; Varki, A. Exploration of sialic acid diversity and biology using sialoglycan microarrays. *Biopolymers* **2013,** *99*, 650-665.

(23) Zhang, Q. W.; Li, Z.; Wang, Y. W.; Zheng, Q.; Li, J. J. Mass spectrometry for protein sialoglycosylation. *Mass Spectrom. Rev.* **2018**, *37*, 652-680.

(24) Nilsson, J.; Ruetschi, U.; Halim, A.; Hesse, C.; Carlsohn, E.; Brinkmalm, G.; Larson, G. Enrichment of glycopeptides for glycan structure and attachment site identification. *Nat. Methods* **2009**, *6*, 809-811.

(25) Bai, H. H.; Fan, C.; Zhang, W. J.; Pan, Y. T.; Ma, L.; Ying, W. T.; Wang, J. H.; Deng, Y. L.; Qian, X. H.; Qin, W. J. A pH-responsive soluble polymer-based homogeneous system for fast and highly efficient N-glycoprotein/glycopeptide enrichment and identification by mass spectrometry. *Chem. Sci.* **2015**, *6*, 4234-4241.

(26) Tian, Y.; Zhou, Y.; Elliott, S.; Aebersold, R.; Zhang, H. Solid-phase extraction of N-linked glycopeptides. *Nat. Protoc.* **2007**, *2*, 334-339.

(27) Zielinska, D. F.; Gnad, F.; Wisniewski, J. R.; Mann, M. Precision mapping of an in vivo N-glycoproteome reveals rigid topological and sequence con-straints. *Cell* **2010**, *141*, 897-907.

(28) Xiao, H.; Chen, W.; Smeekens, J. M.; Wu, R. An enrichment method based on synergistic and reversible covalent interactions for large-scale analysis of glycoproteins. *Nat. Commun.* **2018**, *9*, 1692.

(29) Liu, L. T.; Zhang, Y.; Zhang, L.; Yan, G. Q.; Yao, J.; Yang, P. Y.; Lu, H. J. Highly specific revelation of rat serum glycopeptidome by boronic acid-functionalized mesoporous. *Silica. Anal. Chim. Acta* **2012**, *753*, 64-72.

(30) Xia, C. S.; Jiao, F. L.; Gao, F. Y.; Wang, H. P.; Lv, Y. Y.; Shen, Y. H.; Zhang, Y. J.; Qian, X. H. Two-Dimensional MoS_2-Based Zwitterionic Hydrophilic interaction liquid chromatography material for the specific enrichment of glycopeptides. *Anal. Chem.* **2018**, *90*, 6651-6659.

(31) Jandera, P. Stationary and mobile phases in hydrophilic interaction chromatography: a review. *Anal. Chim. Acta* **2011**, *692*, 1-25.

(32) Larsen, M. R.; Jensen, S. S.; Jakobsen, L. A.; Heegaard, N. H. H. Exploring the sialiome using titanium dioxide chromatography and mass spectrometry. *Mol. Cell. Proteomics* **2007**, *6*, 1778-1787.

(33) Palmisano, G.; Lendal, S. E.; Engholm-Keller, K.; Leth-Larsen, R.; Parker, B. L.; Larsen, M. R. Selective enrichment of sialic acid-containing glycopeptides using titanium dioxide chromatography with analysis by HILIC and mass spectrometry. *Nat. Protoc.* 2010, 5, 1974-1982.

(34) Xiao, H.; Suttapitugsakul, S.; Sun, F.; Wu, R. Mass spectrometry-based chemical and enzymatic methods for global analysis of protein glycosylation. *Acc. Chem. Res.* **2018**, *51*, 1796-1806.

(35) Suttapitugsakul, S.; Sun, F.; Wu, R. Recent advances in glycoproteomic analysis by mass spectrometry. *Anal. Chem.* **2020**, *92*, 267-291.

(36) Gaunitz, S.; Nagy, G.; Pohl, N. L. B. Noyotny, M. V. Recent advances in the analysis of complex glycoproteins. *Anal. Chem.* **2018,** *89, 389-413.*

(37) Chen, C. C.; Su, W. C.; Huang, B. Y.; Chen, Y. J.; Tai, H. C.; Obena, R. P. Interaction modes and approaches to glycopeptide and glycoprotein enrichment. *Analyst* **2014**, *139*, 688-704.

(38) Ongay, S.; Boichenko, A.; Govorukhina, N.; Bischoff, R. Glycopeptide enrichment and separation for protein glycosylation analysis. *J. Sep. Sci.* **2012**, *35*, 2341-2372.

(39) Rowan, S. J.; Cantrill, S. J.; Cousins, G. R. L.; Sanders, J. K. M.; Stoddart, J. F. Dynamic covalent chemistry. *Angew. Chem., Int. Ed.* **2002**, *41*, 898-952.

(40) Siegel, D. Applications of reversible covalent chemistry in analytical sample preparation. *Analyst* **2012**, *137*, 5457-5482.

(41) Vas, G.; Vékey, K. Solid-phase microextraction: a powerful sample preparation tool prior to mass spectrometric analysis. *J. Mass Spectrom.* **2004**, *39*, 233-254.

(42) Xue, Y.; Xie, J. J.; Fang, P.; Yao, J.; Yan, G. Q.; Shen, H. L.; Yang, P. Y. Study on behaviors and performances of universal N-glycopeptide enrichment methods. *Analyst* **2018**, *143*, 1870-1880.

(43) Qing, G. Y.; Li, X. L.; Xiong, P.; Chen, C.; Zhan, M. M.; Liang, X. M.; Sun, T. L. Dipeptide-based carbohydrate receptors and polymers for glycopeptide enrichment and glycan discrimination. *ACS Appl. Mater. Interfaces,* **2016**, *8*, 22084-22092.

(44) Li, X. L.; Xiong, Y. T.; Qing, G. Y.; Jiang, G.; Li, X. Q.; Sun, T. L.; Liang, X. M. Bioinspired saccharide-saccharide interaction and smart polymer for specific enrichment of sialylated glycopeptides. *ACS Appl. Mater. Interfaces*, **2016**, 8, 13294-13302.

(45) Dong, X. F.; Qin, H. Q.; Mao, J. W.; Yu, D. P.; Li, X. L.; Shen, A. J.; Yan, J. Y.; Yu, L.; Guo, Z. M.; Ye, M. L.; Zou, H. F.; Liang, X. M. In-depth analysis of glycoprotein sialylation in serum using a dual-functional material with superior hydrophilicity and switchable surface charge. *Anal. Chem.* **2017**, *89*, 3966-3972.

(46) Wang, Y. L.; Liu, M. B.; Xie, L. Q.; Fang, C. Y.; Xiong, H. M.; Lu, H. J. Highly Efficient Enrichment Method for Glycopeptide

Analyses: Using specific and nonspecific nanoparticles synergistically. *Anal. Chem.* **2014**, *86,* 2057-2064.

(47) Cao, Q. C.; Ma, C.; Bai, H. H.; Li, X. Y.; Yan, H.; Zhao, Y.; Ying, W. T.; Qian, X. H. Multivalent hydrazide-functionalized magnetic nanoparticles for glycopeptide enrichment and identification. *Analyst* **2014**, *139*, 603-609.

(48) Chen, Y.; Ding, L.; Ju, H. In situ cellular glycan analysis. *Acc. Chem. Res.* **2018**, *51*, 890-899.

(49) Herrmann, A. Dynamic Mixtures: Challenges and opportunities for the amplification and sensing of scents. *Chem.-Eur. J.* **2012**, *18*, 8568-8577.

(50) Delort, E.; Darbre, T.; Reymond, J. L. A strong positive dendritic effect in a peptide dendrimer-catalyzed ester hydrolysis reaction. *J. Am. Chem. Soc.* **2004**, *126,* 15642-15643.

(51) Yabe, R.; Suzuki, R.; Kuno, A.; Fujimoto, Z.; Jigami, Y.; Hirabayashi, J. Tailoring a novel sialic acid-binding lectin from a ricin-B chain-like galactose-binding protein by natural evolution-mimicry. *J. Nutr. Biochem.* **2007,** *141*, 389-399.

(52) Wei, J.; Shen, A. J.; Wan, H. H.; Yan, J. Y.; Yang, B. C.; Guo, Z. M.; Zhang, F. F.; Liang, X. M. Highly selective separation of aminoglycoside antibiotics on a zwitterionic Click TE-Cys column. *J. Sep. Sci.* **2014**, *37*, 1781-1787.

(53) Hassib, H. B.; Abdel-Kader, N. S.; Issa, Y. M. Kinetic study of the hydrolysis of schiff bases derived from 2-Aminothiophenol. *J. Solution Chem.* **2012**, *41*, 2036–2046

(54) Birchall, L. S.; Roy, S.; Jayawarna, V.; Hughes, M.; Irvine, E.; Okorogheye, G. T.; Saudi, N.; De Santis. E.; Tuttle, T.; Edwards, A. A. Exploiting CH-π interactions in supramolecular hydrogels of aromatic carbohydrate amphiphiles. *Chem. Sci.* **2011**, *2*, 1349-1355.

(55) Panja, A.; Ghosh, K. Exploiting 4-Hydroxybenzaldehyde derived Schiff base gelators: case of the sustainability or rupturing of imine bonds towards the selective sensing of Ag^{+} and Hg^{2+} ions via sol-gel methodology. *New J. Chem.* **2019**, *43*, 5139-5149.

(56) Gosecka, M., Urbaniak, M., Mikina, M., Gosecki, M., and Rozanski, A. Homodimerization driven self-assembly of glycoluril molecular clips with covalently immobilized poly(epsilon-caprolactone). *Soft Matter* **2018**, *14*, 7945-7949.

(57) Lee, P. H.; Gao, A.; van Staden, C.; Ly, J.; Salon, J.; Xu, A.; Fang, Y.; Verkleeren, R. Evaluation of dynamic mass redistribution technology for pharmacological studies of recombinant and endogenously expressed G protein-coupled receptors. *Assay Drug Dev. Technol.* **2008**, *6*, 83-94.

(58) Xu, Z.; Chen, X.; Liu, J.; Yan, D. Q.; Diao, C. H.; Guo, M. J.; Fan, Z. Self-assembly behavior of tail-to-tail superstructure formed by mono-6-O-(4-carbamoylmethoxy-benzoyl)-β-cyclodextrin in solution and the solid state. *Carbohydr. Res.* **2004**, *393*, 32-36.

(59) Jiang, H.; Hu, W. L.; Li, J. G.; Yang, G.; Zou, G.; Zhang, Q. J. Tunable morphology and surface wettability of an amphiphilic azobenzene derivative and its melamine-induced self-assembly. *Supramol. Chem.* **2015**, *27*, 181-190.

(60) Brisson, E. R. L.; Xiao, Z. Y.; Franks, G. V.; Connal, L. A. Versatile synthesis of amino acid functional polymers without protection group chemistry. *Biomacromolecules* **2017**, *18*, 272-280.

(61) Belowich, M. E.; Stoddart, J. F. Dynamic imine chemistry. *Chem. Soc. Rev.* **2012**, *41*, 2003-2024.

(62) Qing, G.; Yan, J.; He, X.; Li, X.; Liang, X. Recent advances in hydrophilic interaction liquid interaction chromatography materials for glycopeptide enrichment and glycan separation. *TrAC, Trends Anal. Chem.* **2020**, *124*, 115570.

(63) Philbrook, A.; Blake, C. J.; Dunlop, N.; Easton, C. J.; Keniry, M. A.; Simpon, J. S. Demonstration of co-polymerization in melamine-urea-formaldehyde reactions using ^{15}N NMR correlation spectroscopy. *Polymer* **2005,** *46*, 2153-2156.

(64) Hassib, H. B.; Abdel-Kader, N. S.; Issa, Y. M. Kinetic study of the hydrolysis of schiff bases derived from 2-aminothiophenol. *J. Solution Chem.* **2012**, *41*, 2036-2046.

(65) Xie, D.; Zhu W. F.; Cheng, H.; Yao, Z. Y.; Li, M.; Zhao, Y. L. An antibody-free assay for simultaneous capture and detection of glycoproteins by surface enhanced raman spectroscopy. *Phys. Chem. Chem. Phys.* **2018**, *20*, 8881-8886.

(66) Sun, F.; Bai, T.; Zhang, L.; Ella-Menye, J. R.; Liu, S. J.; Nowinski, A. K.; Jiang, S. Y.; Yu, Q. M. Sensitive and fast detection of fructose in complex media via symmetry breaking and signal amplification using surface-enhanced raman spectroscopy. *Anal. Chem.* **2014**, *86*, 2387-2394.

(67) Otsuka, H.; Uchimura, E.; Koshino, H.; Okano, T.; Kataoka, K. Anomalous binding profile of phenylboronic acid with N-acetylneuraminic acid (Neu5Ac) in aqueous solution with varying pH. *J. Am. Chem. Soc.* **2003**, *125*, 3493-3502.

(68) Chiş, V.; Venter, M. M.; Leopold, N.; Cozar, O. Raman, surface-enhanced raman scattering and DFT study of para-nitro-aniline. *Vib. Spectrosc.* **2008**, *48*, 210-214.

(69) Prins, L. J.; Scrimin, P. Covalent Capture: Merging Covalent and Noncovalent Synthesis. *Angew. Chem., Int. Ed.* **2009**, *48*, 2288-2306.

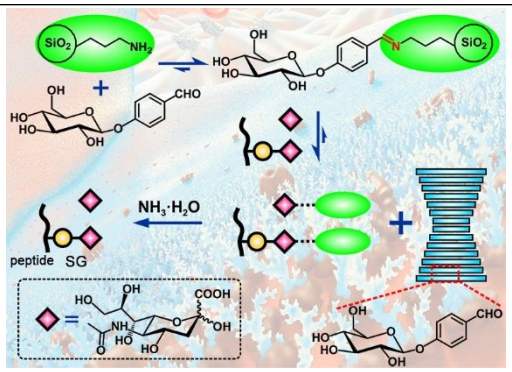

Table of Contents artwork

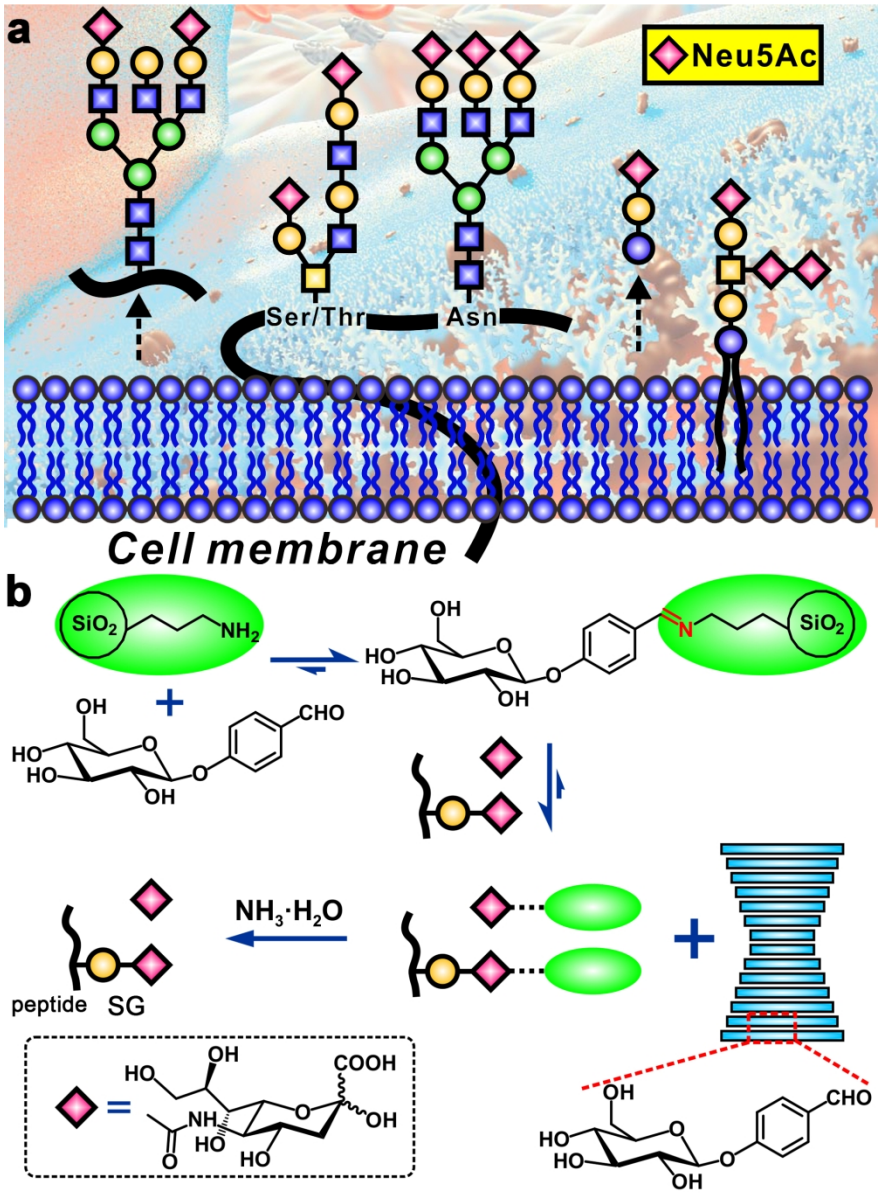
a
Neu5Ac
Ser/Thr
Asn
Cell membrane
b
SiO2
NH2
OH
HO
HO
O
OH
N
SiO2
OH
HO
HO
O
OH
CHO
NH3·H2O
peptide
SG
HO
OH
COOH
NH
HO
HO
O
OH
OH
HO
HO
O
OH
CHO

Figure 1

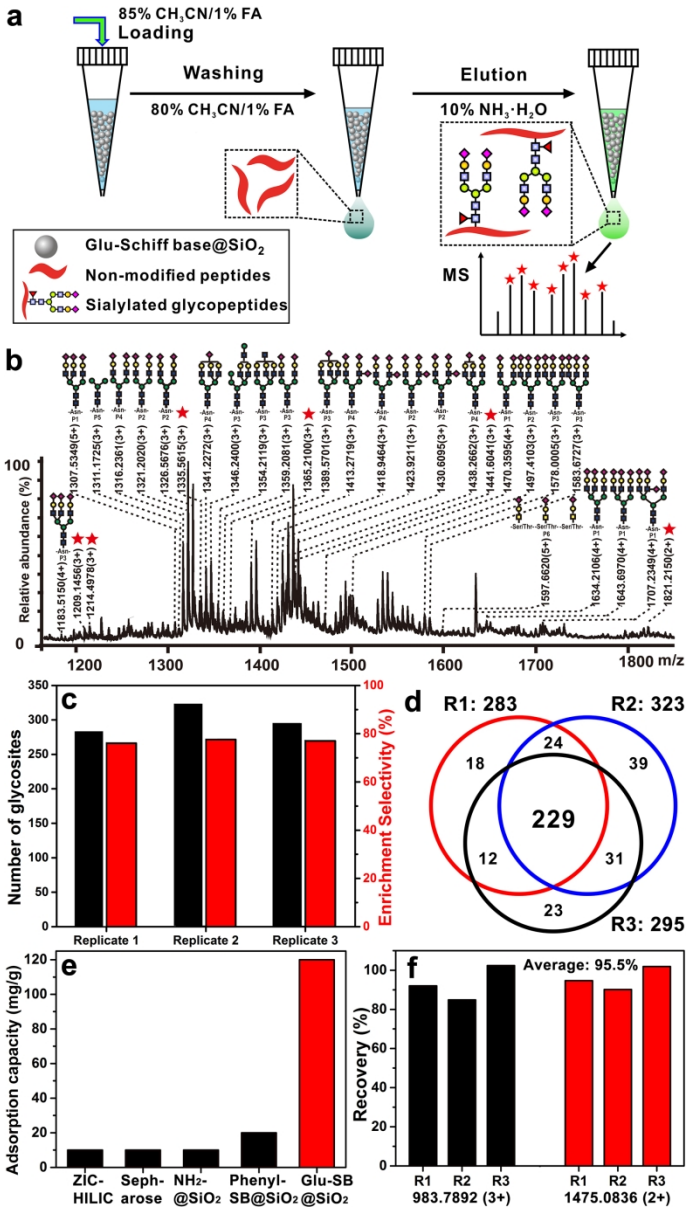
a
85% CH3CN/1% FA
Loading
Washing
80% CH3CN/1% FA
Elution
10% NH3·H2O
Glu-Schiff base@SiO2
Non-modified peptides
Sialylated glycopeptides
MS
b
Relative abundance (%)
m/z
c
Number of glycosites
Enrichment Selectivity (%)
Replicate 1
Replicate 2
Replicate 3
d
R1: 283
R2: 323
R3: 295
24
18
39
229
12
31
23
e
Adsorption capacity (mg/g)
ZIC-HILIC
Seph-arose
NH2-@SiO2
Phenyl-SB@SiO2
Glu-SB@SiO2
f
Recovery (%)
Average: 95.5%
R1
R2
R3
983.7892 (3+)
1475.0836 (2+)

Figure 2

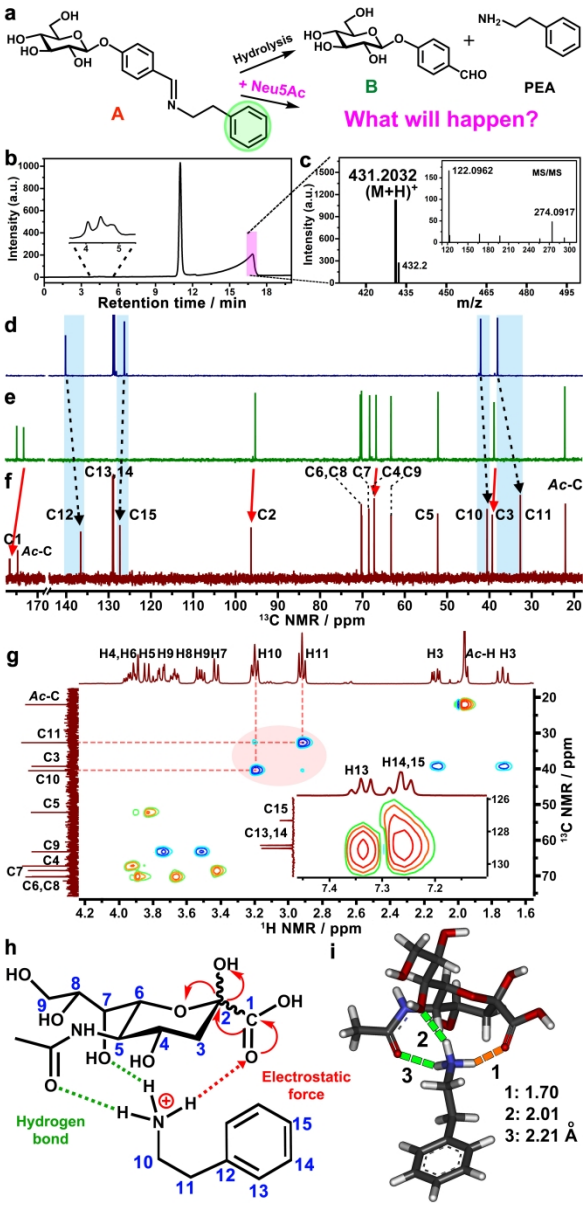
a
Hydrolysis
+ Neu5Ac
A
B
PEA
What will happen?
b
Intensity (a.u.)
Retention time / min
c
431.2032
(M+H)+
432.2
122.0962
MS/MS
274.0917
m/z
d
e
f
C13,14
C12
C15
C2
C6,C8 C7
C4,C9
C5
C10
C3
C11
Ac-C
C1
13C NMR / ppm
g
H4,H6,H5,H9,H8,H9,H7
H10
H11
H3
Ac-H H3
H13
H14,15
C15
C13,14
1H NMR / ppm
h
Electrostatic force
Hydrogen bond
i
1: 1.70
2: 2.01
3: 2.21 Å

Figure 3

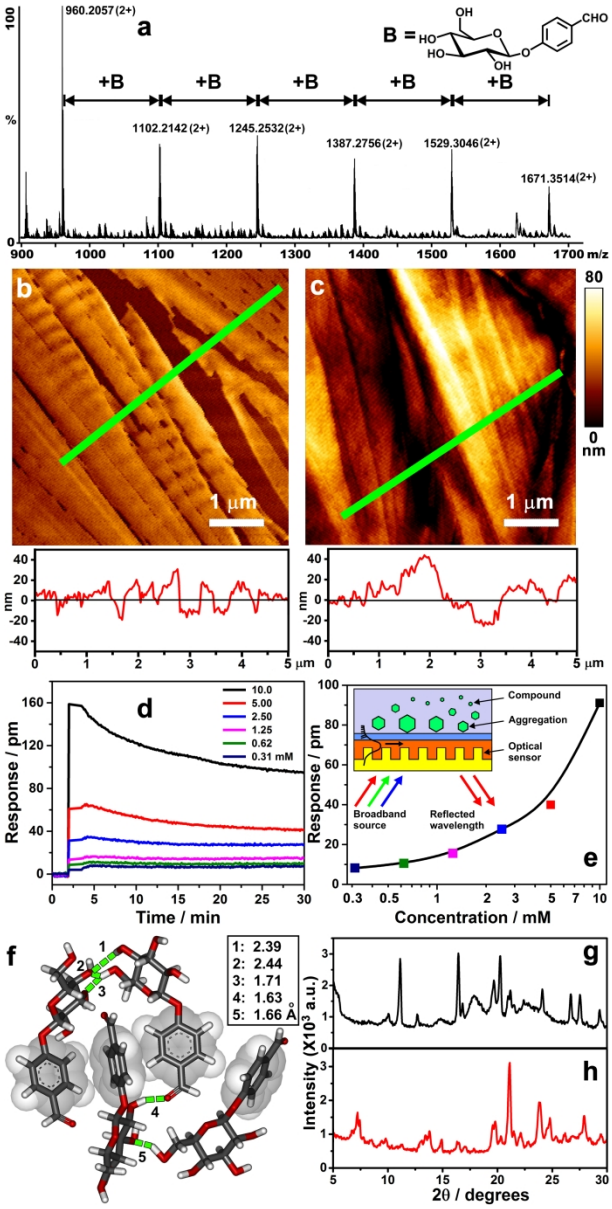
a
960.2057(2+)
B =
+B
1102.2142(2+)
1245.2532(2+)
1387.2756(2+)
1529.3046(2+)
1671.3514(2+)
m/z
b
c
1 μm
80
0
nm
d
Response / pm
Time / min
10.0
5.00
2.50
1.25
0.62
0.31 mM
e
Compound
Aggregation
Optical sensor
Broadband source
Reflected wavelength
Concentration / mM
f
1: 2.39
2: 2.44
3: 1.71
4: 1.63
5: 1.66 Å
g
h
Intensity (X10³ a.u.)
2θ / degrees

Figure 4

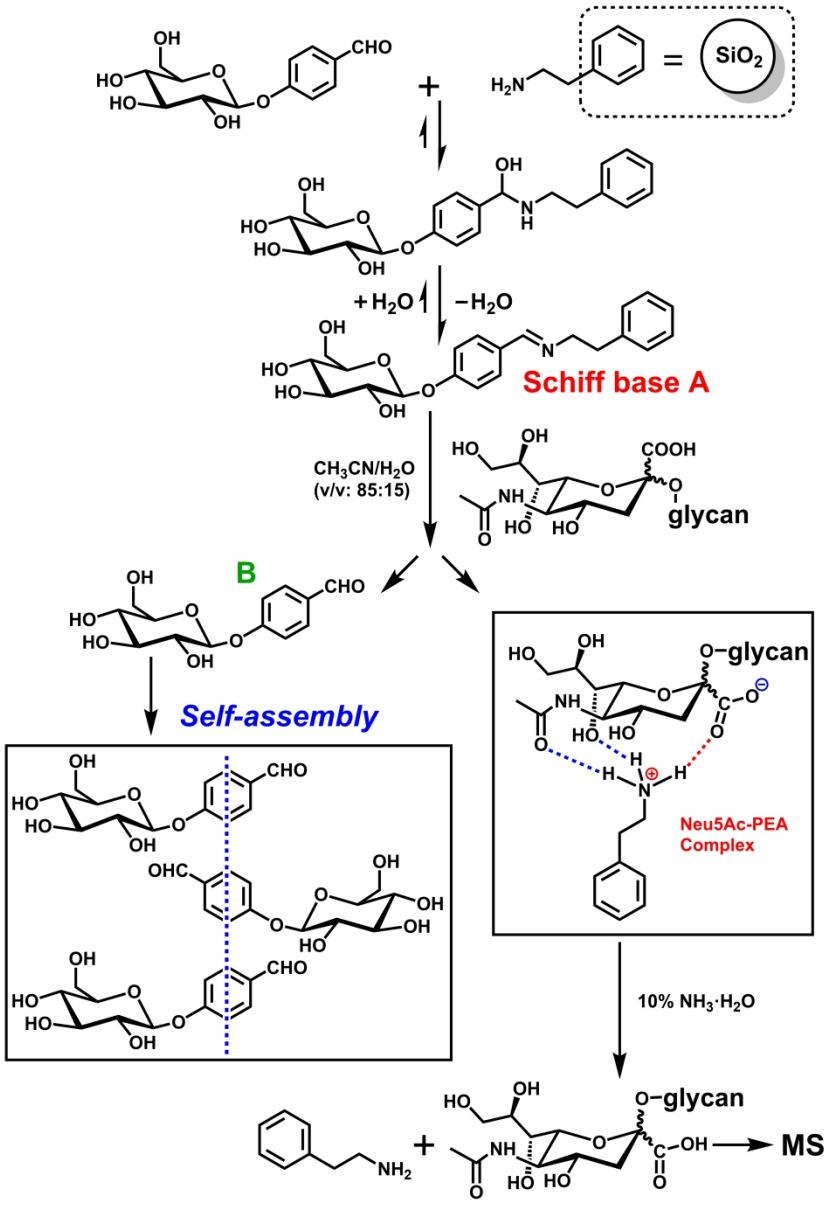

Figure 5

158x228mm (600 x 600 DPI)

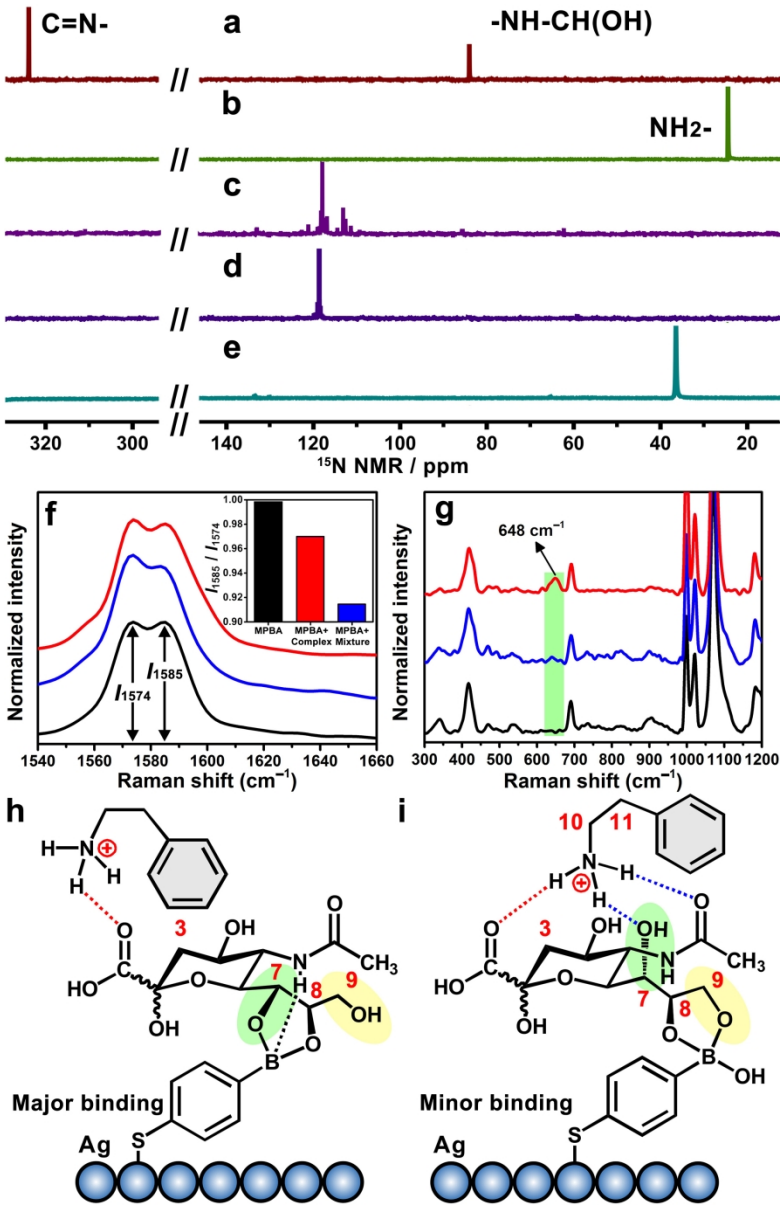
C=N-
a
-NH-CH(OH)
b
NH2-
c
d
e
320
300
140
120
100
80
60
40
20
15N NMR / ppm
f
Normalized intensity
I1585 / I1574
MPBA
MPBA+ Complex
MPBA+ Mixture
I1574
I1585
Raman shift (cm−1)
g
648 cm−1
Normalized intensity
Raman shift (cm−1)
h
Major binding
Ag
i
Minor binding
Ag

Figure 6